Investigation of heat transfer in turbulent nanofluids using direct numerical simulations

Sasidhar Kondaraju,[1,2] E. K. Jin,[3] and J. S. Lee[4,*]
[1]*Department of Mechanical Engineering, Wayne State University, Detroit, Michigan 48202, USA*
[2]*Department of Aerospace and Mechanical Engineering, University of Arizona, Tucson, Arizona 85721, USA*
[3]*Department of Atmospheric, Ocean and Earth Science, George Mason University, Fairfax, Virginia 22030, USA*
[4]*Department of Mechanical Engineering, Yonsei University, Seoul, Korea*
(Received 13 August 2009; revised manuscript received 7 November 2009; published 11 January 2010)

A numerical study has been performed by using a combined Euler and Lagrangian method on the convective heat transfer of Cu and Al_2O_3 nanofluids under the turbulent flow conditions. The effects of volume fraction of nanoparticles, nanoparticle sizes, and nanoparticle material are investigated. The mechanism of convective heat transfer enhancement in nanofluids has also been investigated, by studying the influence of particle dispersion and two-way interaction between fluid and particle temperature. The results show significant enhancement of heat transfer of nanofluids. The numerical data are compared with the correlation data of the experiments and reasonably good agreement is achieved.

DOI: 10.1103/PhysRevE.81.016304 PACS number(s): 47.61.−k, 47.27.E−, 44.35.+c

I. INTRODUCTION

With technological developments in thermal engineering and thermoscience, which have very high thermal load and require sophisticated cooling technologies, many efforts have been devoted to heat transfer enhancement. Among the various methods investigated to improve the heat transfer, suspension of nanoparticles in liquid gained considerable interest among researchers ever since Choi [1] stably suspended nanoparticles in liquid and showed an improved thermal conductivity in these new solid-liquid suspensions. He termed this new fluid as nanofluids, where nanoparticles with at least one of their dimensions smaller than about 100 nm are suspended in liquid medium.

Over the years, researchers have extensively studied the thermal conductivity of nanofluids, and they found an anomalous increase in the thermal conductivity even at low volume concentrations ($\Phi < 5\%$) of suspended nanoparticles [2–7]. To explain the reasons for the anomalous increase in the thermal conductivity of nanofluids, based on the experimental [2–4,6,8] and theoretical studies [9–12], three main possible mechanisms were suggested: dispersion of nanoparticles, the nature of heat transport in nanoparticles, and the effects of nanoparticles clustering. Dispersion of nanoparticles alters the fluid composition and affects the energy transport process in the nanofluids; thus influencing the effective thermal conductivity of nanofluids [11,12]. Jang and Choi [13], for the first time, developed a dynamic model that includes the convection induced by the Brownian motion of nanoparticles. They indicated that the Brownian motion produces convection like effects at the nanoscale; it therefore enhances the thermal conductivity of nanofluids. They also suggested that the decreasing nanoparticle size increases the thermal conductivity in nanofluids due to the enhancement of the Brownian force at reduced particle sizes. However, Murshed *et al.* [14] argued that the model assumed macroscale convection behavior at the nanoscale by invoking macroscale correlations for flow around a solid sphere. Nie *et al.* [15] indicated that the enhancement of thermal conductivity due to the Brownian motion of particles is less than 5%. Murshed *et al.* [5] and Eastman *et al.* [9] showed that the interfacial interactions among the particles and liquid enhance energy transport inside the liquid and also effects heat transport in nanoparticles. It was, experimentally by Zhu *et al.* [7] and numerically by Xuan and Li [10], shown that the clustering of nanoparticles affects the effective thermal conductivity of nanofluids negatively. Though various theoretical models were proposed to understand the effective thermal conductivity of nanofluids, all models are usually applicable to limited data. The present authors, Kondaraju *et al.*[16] using the model presented in this paper, have previously shown that all three mechanisms discussed above have significant effect on the increase of the thermal conductivity of nanofluids (the paper has been accepted by Int. J. Heat Mass Transfer).

For applying nanofluids in practical uses, it is necessary to move beyond static thermal conductivity measurements to explore the convective heat transfer behavior of nanofluids. However, it is noticed that very few publications have dealt with the convective heat transfer of nanofluids. Experiments carried out to measure the convective heat transfer coefficient of nanofluids, in both turbulent and laminar regimes, indicated the dependence of Nusselt number on the various properties of nanofluids, e.g., the volume fraction of nanofluids, density of nanoparticles and base fluids [17–19]. Maiga *et al.* [20,21] performed numerical simulations to study the convective heat transfer in nanofluids by assuming the nanofluid as a single phase fluid. They adopted the nanofluid as a single phase fluid with changed physical parameters such as density, thermal conductivity, and viscosity in the single phase flow method. The physical properties of nanofluids (density, thermal conductivity, and viscosity) were predicted by assuming that the nanoparticles were well dispersed in the base fluid. He *et al.* [22] studied the convective heat transfer of TiO_2 nanofluids under the laminar conditions using an Eulerian-Lagrangian two-phase model. Due to the direct interaction of particles with fluid medium, the assumptions made in single phase models are no longer necessary while using this model. However, He *et al.* [22] did not con-

*Corresponding author. joonlee@yonsei.ac.kr

sider the van der Waals force between nanoparticles, thus neglecting the coagulation of nanoparticles in the fluid. They also neglected the two-way temperature coupling effects between particles and fluid.

All the above mentioned papers reported the effects of different properties of nanofluids (i.e., volume fraction of nanofluids, density of nanoparticles, and Reynolds number of fluid) on the Nusselt number of nanofluids. But these papers failed to mention the mechanism of increase in heat transfer in nanofluids. In this paper, the authors examine the effects of volume fraction of nanofluids and size of nanoparticles on the convective heat transfer in nanofluids. While a fair amount of study has been performed to understand the effects of Brownian motion and thermal transport in nanoparticles on thermal conductivity of nanofluids, no such study has been performed to understand the increase in convective heat transfer in nanofluids. The authors will try to understand the effect of these phenomena in the present paper.

To perform the numerical simulations, multiphase Navier-Stokes equations has been used, where fluid phase was solved using Eulerian frame and particle phase was solved using Lagrangian frame of reference. Three possible mechanisms, dispersion of nanoparticles, the nature of heat transport in nanoparticles, and the effects of nanoparticles clustering, responsible for the anomalous increase in the thermal conductivity of nanofluids, were modeled as different terms in the nanoparticle momentum and temperature equations. Dispersion of nanoparticles was taken care by applying forces such as the Brownian force, thermophoresis force and van der Waals force in the nanoparticle momentum equation. The coagulation of nanoparticles was also controlled by the van der Waals force acting on the adjacent nanoparticles. Interfacial interaction between particles and liquid was modeled by an addition of a temperature source term to the fluid temperature equation.

The authors, Kondaraju *et al.* [23], had previously developed a two-phase flow model to study the dispersion of solid particle in fluid medium. Here the authors extended the model to account for the nanoparticle forces acting on the particles and suspension of multisized particles in the fluid medium. Details of mathematical and numerical models are provided in the next section followed by the discussion of the present results.

II. MATHEMATICAL MODEL

Nanoparticles used in the simulations are characterized by an aerodynamic and thermal response time. The particles have no volume displacement, so it is impossible for a particle to occupy more than one computational cell at any instance of time. Thus interpolation has been performed to obtain the fluid velocities at the particle positions. While performing the fluid interpolation, a proper grid length has to be chosen to ensure accurate interpolations. Method of choosing grid length has been discussed in the section "Numerical methods and flow conditions." Fluid interpolation cell corresponding to a particle is obtained by dividing the particle coordinates with the grid spacing. When particles land precisely at the domains of $x_j=2\pi$, where $j=1,2,3$, particles were considered to have exited the flow domain and were therefore wrapped around the opposite domain boundary before performing the fluid interpolation. The details of particle and fluid equations are given below.

In the Lagrangian frame of reference, the equation of motion of nanoparticle and time dependent particle temperature equation are given by

$$(dx_i^n)/dt \equiv v_i^n, \tag{1}$$

$$\frac{dv_i}{dt} = F_{Di} + F_{Bi} + F_{Ti} + F_{Vi}, \tag{2}$$

$$\frac{dT_p}{dt} = \frac{\mathrm{Nu}}{\tau_T}\frac{(\theta_f - T_p)}{2}, \tag{3}$$

where x_i^n and v_i^n v_p are the instantaneous particle position and velocity of the nth particle, respectively. Subscript i represents the tensor notation. τ_T is thermal response time of the particle and given as $\tau_T=\frac{\rho_p c_p d_p^2}{12k_f}$. k_f, d_p, c_p, and ρ_p are the nanoparticle thermal conductivity of the base fluid, diameter, specific heat and density of the particle, respectively. Nu is the Nusselt number, which is calculated using Ranz-Marshall correlation.

$$\mathrm{Nu} = 2 + 0.6\ \mathrm{Re}_p^{1/2}\ \mathrm{Pr}^{1/3}, \tag{4}$$

$\mathrm{Re}_p^{1/2}$ is the particle Reynolds number and is calculated in the above equation using $d_p/2$ as the characteristic length. θ_f is the fluid fluctuation temperature in the neighborhood of the particle and T_p is the temperature of the particle.

F_{Di} is the hydrodynamic drag force from the fluid, which is calculated by applying the Stokes law [24]

$$F_{Di} = \frac{1}{\tau_p}[u_i(x_i^n) - v_i^n], \tag{5}$$

$$\tau_p = \frac{\rho_p d_p^2}{18\nu\rho_f}, \tag{6}$$

τ_p is the particle aerodynamic response time. u is the fluid velocity in the neighborhood of the particle, ρ_f is the fluid density and ν is the kinematic viscosity of fluid. The values of relaxation times τ_p and τ_T are calculated relative to the Kolmogorov time scale and are found to be equal to $\tau_p/\tau_k = 3.384\times10^{-3}$ and $\tau_T/\tau_k = 6.439\times10^{-3}$, respectively. Here τ_k is the Kolmogorov time scale. Also the diameter of the particle is comparatively smaller than the Kolmogorov length scale $(d_p/\eta=0.04)$ thus indicating that the particles are entrained in the fluid turbulent eddies.

The Brownian force F_{Bi} [25] is given as in Eq. (2).

$$F_{Bi} = G_i\left(\frac{216}{\pi}\frac{\nu k_B T}{\rho_f d_p^5\left(\frac{\rho_p}{\rho_f}\right)^2 C_c \Delta t}\right)^{1/2} \tag{7}$$

G_i is the Gaussian random number with zero mean and unit variance. C_c is known as the Cunningham correction factor. k_B is the Boltzmann constant and T is the initial temperature

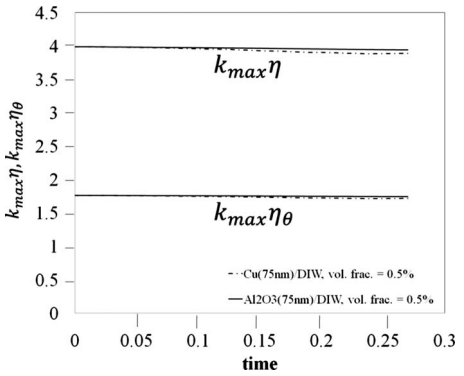

FIG. 1. Temporal evolution of $k_{\max}\eta$ and $k_{\max}\eta_\theta$ along time is shown in the plot. Values of $k_{\max}\eta$ and $k_{\max}\eta_\theta$ are always greater than one, thus ensuring accurate resolution of small scale structures and accurate interpolation of fluid velocities.

of fluid. k_BT is known as the thermal energy and at room temperature $(0.4\times10^{-20}$ J).

The contribution of thermophoretic effect [26] F_{Ti} in Eq. (2) can be given by

$$\boldsymbol{F_T} = -\frac{6\pi d_p \nu^2 C_s (k_r + 2.18\ \mathrm{Kn})}{\rho(1+3\times1.14k_r)(1+2k_r+4.36\ \mathrm{Kn})}\frac{1}{m_p T}\frac{\partial T_f}{\partial \boldsymbol{x}_i}. \tag{8}$$

Though the thermophoretic force has been first proposed for particles suspended in gas, McNab and Meisen [27] had proposed a formula similar to one used by authors while formulating the thermophoretic force equation for 1 μm particles suspended in water and *n*-hexane. The equation was later also proposed as a thermophoretic force acting on nanoparticles suspended in liquids by Das *et al.* [28]. In Eq. (8), k_r is the thermal conductivity ratio of nanoparticle to base fluid. Kn is the Knudsen number defined as $\mathrm{Kn}=\frac{2\lambda}{d_p}$ where λ is the mean free path of the fluid molecule. $C_s(=1.147)$ is the thermal slip coefficient and $\frac{\partial T_f}{\partial x_i}$ is the temperature gradient of fluid in the x_i direction. m_p is mass of the nanoparticle.

The van der Waals force, F_{vi} is approximated as Casimir effect [29] and is given as

$$F_{vi} = \frac{A d_{p1} d_{p2}}{12(d_{p1}+d_{p2})h_i^2}\delta, \tag{9}$$

where d_{p1} and d_{p2} are diameters of two individual nanoparticles with a distance h between them. A is called as Hamaker constant and is of order of 10^{-19} J [29]. δ is called the London retardation wavelength and is set to 100 nm. As particles come in contact, Eq. (8) predicts that the colloidal force is infinite because h reduces to zero. In order to prevent singularity as h reduces to zero in the solution, a cutoff distance of 0.2 nm was implemented in the calculations based on the relative magnitudes of all the forces acting on the particles. When particles are closer than the cutoff distance, particles are allowed to coagulate and a new diameter is calculated based on the sum of two coagulated particle diameters.

TABLE I. The simulated cases, used for the study the effect of the volume fraction of nanofluids on the convective heat transfer of nanofluids, are shown.

Material	Particle diameter (d) (nm)	Volume fractions (Φ)
Cu	100	0.1%, 0.5%, 1.0%
Al_2O_3	100	0.1%, 0.5%, 1.0%

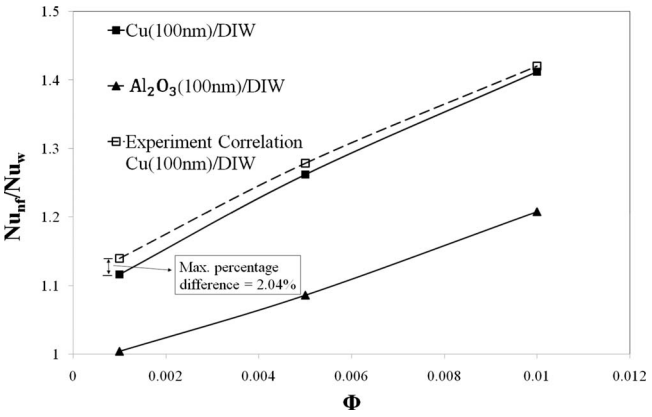

FIG. 2. Effective Nusselt number of Cu(100)/DIW and Al_2O_3(100 nm)/DIW nanofluids are plotted at different volume fractions. Effective Nusselt number is observed to increase with the increase of the volume fraction of nanofluids.

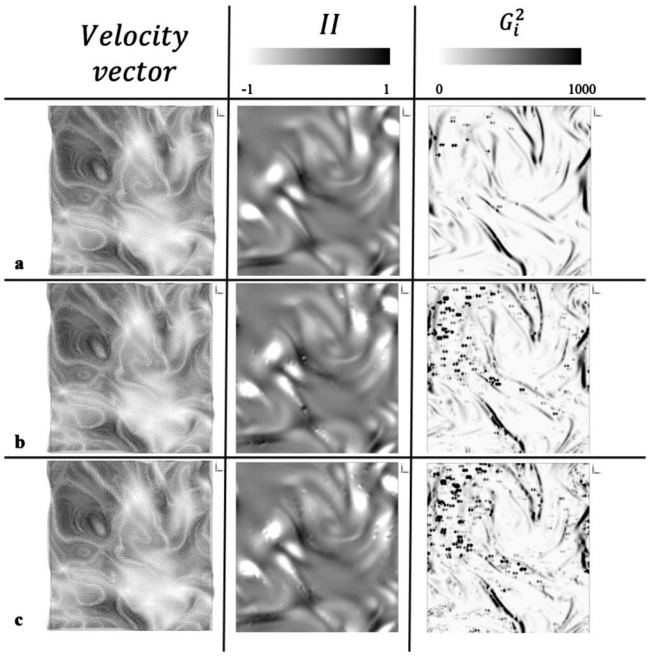

FIG. 3. Contours of instantaneous velocity vector, deformation tensor II and square temperature gradient G_i^2 are shown for Cu(100 nm)/DIW nanofluids at different volume fractions. (a) Cu(100 nm)/DIW nanofluid at $\Phi=0.5\%$; (b) Cu(100 nm)/DIW nanofluid at $\Phi=0.1\%$; (c) Cu(100 nm)/DIW nanofluid at $\Phi=1.0\%$. Change in the values of II with the change of the volume fraction of nanofluids is observed to be negligible. However, the contour plot of G_i^2 shows a significant increase in its values as the volume fraction of nanofluids increases.

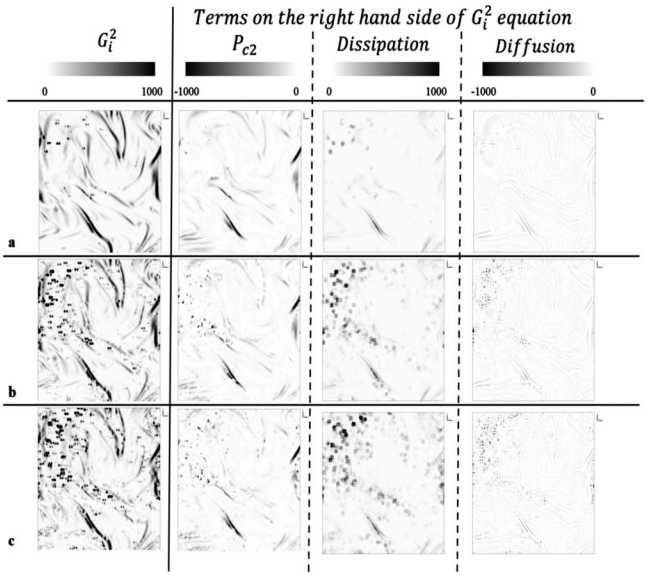

FIG. 4. Distribution of G_i^2 and the terms in the G_i^2 evolution equation; P_{c2}, dissipation and dissipation are shown for (a) Cu(100 nm)/DIW nanofluids at $\Phi=0.1\%$; (b) Cu(100 nm)/DIW nanofluid at $\Phi=0.5\%$; (c) Cu(100 nm)/DIW nanofluid at $\Phi=1.0\%$. The contour of G_i^2 shows a significant increase in its values at volume fraction of 1.0%.

Time-dependent, three-dimensional Navier-Stokes equations are solved in a cubical domain with the periodic boundary condition. The nondimensional equations for fluid can be expressed as

$$\frac{\partial \hat{u}_i}{\partial t} + \hat{u}_j \hat{u}_{i,j} = -\hat{p}_{,i} + \frac{1}{\mathrm{Re}} \hat{u}_{i,jj} + Q\hat{u}_i - \hat{F}_{pi}, \tag{10}$$

$$\hat{u}_{i,i} = 0, \tag{11}$$

$$\frac{\partial \hat{\theta}_f}{\partial t} + \hat{u}_j \frac{\partial \hat{\theta}_f}{\partial x_i} = -\frac{1}{\mathrm{Re\ Pr}} \frac{\partial^2 \hat{\theta}_f}{\partial x_j^2} + \hat{u}_2 \bar{\nabla} T + \hat{q}_{2w}. \tag{12}$$

The cap "$\hat{\cdot}$" is used in the Eqs. (10)–(12), indicating that the values used here are nondimensionalized. This model, which is often called as homogeneous thermal convection model assumes that the temperature field can be decomposed into the fluctuating part $\hat{\theta}_f$ subjected to periodic boundary conditions and the constant mean part T_o. $\bar{\nabla} T$ in Eq. (11) denotes the mean temperature gradient in the x_2 direction, which effectively acts as a source term for the fluid temperature field. The nondimensional value of $\bar{\nabla} T$ is taken as 1.0 in the present simulations. Similar studies of homogeneous thermal convection have been carried out previously to examine the relation between turbulent flow and heat transfer [30–33]. The system considered here is a reasonable model for a turbulent convection in the regions with approximately constant mean temperature gradient far from the walls, e.g., reverse flow combustion chambers, fan less convection cooling for personal computers. This model decouples complicated boundary layer physics from the thermal convection far from the wall. Thus the study will help in understanding the physics behind the enhancement of convection heat transfer in nanofluids without worrying about the boundary layer physics. Another advantage of the system is the possibility of utilizing an effective numerical simulation.

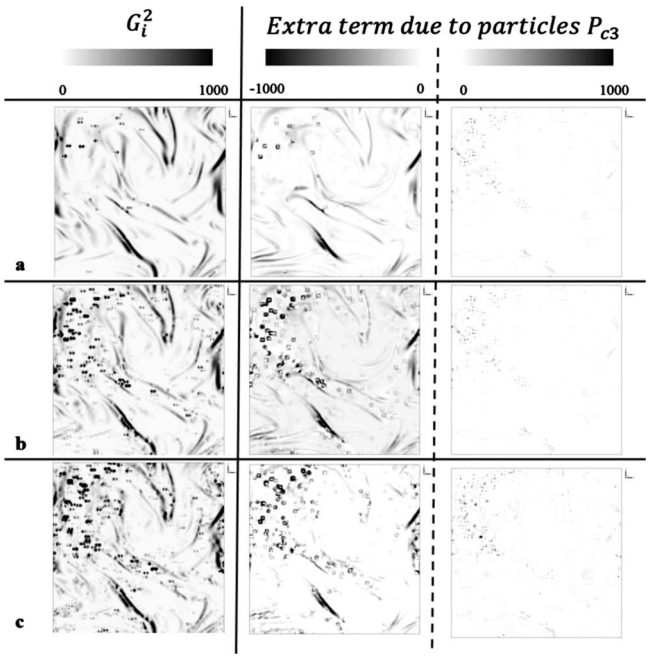

FIG. 5. Distribution of G_i^2 and the negative and positive terms of P_{c3} are shown for (a) Cu(100 nm)/DIW nanofluids at $\Phi=0.1\%$; (b) Cu(100 nm)/DIW nanofluid at $\Phi=0.5\%$; (c) Cu(100 nm)/DIW nanofluid at $\Phi=1.0\%$. Distribution of positive value of P_{c3} is very small and is not significantly influenced by the change of the volume fraction. However, the negative value of P_{c3} is found to be significantly increased with the increase of the volume fraction of nanofluids.

Other parameters used in Eqs. (10)–(12) are as follows. u is velocity of the fluid, p is pressure field, Re is the Reynolds number and Pr is the Prandtl number. Subscripts i and j represent tensor notations; and subscripts ", i" and ", j" represent differentiation with respect to x_i and x_j, respectively. Q is the linear forcing applied in the momentum equation to obtain a stationary isotropic turbulence. The method followed to obtain the stationary isotropic turbulent flow is identical to the method followed by Rosales and Meneveau [34]. The linear forcing coefficient used in the present simulations was $Q=0.0667$. Stationary turbulence was obtained at Taylor's Reynolds number of 33.01. The Prandtl number in the present model was taken as 5.1028, which is the Prandtl number of water at 300 K.

F_{pi} is the net force exerted by the particles on fluid and is shown in Eq. (13) [35]. N_p is the total number of particles in the computational domain. $\delta(x-x^n)$ is the Dirac delta function. v^n is the velocity of nth particle and $u(x^n)$ is the velocity of fluid at the position of the nth particle. Though the two-way coupling effects of the Brownian force and thermophoretic force are not directly included into the particle momentum source term, velocity of the particle used for the two-way coupling interaction is collected after the updating the forces acting on the particles. Thus, the two-way cou-

TABLE II. The normalized spatial average values of G_i^2, P_{c2} and P_{c3}, are shown here for different volume fractions of Cu(100 nm)/DIW nanofluids. The spatial average values of G_i^2 and P_{c3} are observed to be increasing and the spatial average values of P_{c2} are found to be decreasing with the increase of the volume fraction of nanofluids.

Cu(100 nm)/DIW nanofluid volume fraction percentage (Φ)	$\langle G_i^2\rangle/(\langle G_i^2\rangle)_{0.1\%}$	$\langle P_{c2}\rangle/(\langle P_{c2}\rangle)_{0.1\%}$	$\langle P_{c3}\rangle/(\langle P_{c3}\rangle)_{0.1\%}$
0.1	1	1	1
0.5	1.223	0.949	3.416
1.0	1.335	0.919	9.129

pling effect of Brownian force and thermophoretic force are indirectly accommodated into the particle source term.

$$F_{pi} = \frac{1}{\rho_f}\sum_{n=1}^{N_p}\frac{m_p[u(x^n)-v^n]}{\tau_p}\delta(x-x^n). \tag{13}$$

As indicated in the introduction, the authors use a temperature coupling term, q_{2w}, to couple particle temperature source to the fluid temperature equation. This term, similar to momentum coupling term, is introduced into the model as a point source. The source term q_{2w} arises because of the convective heat transfer to and from the particle. The coupling term is calculated by applying the action-reaction principle to a generic volume of fluid (here considered as a grid cell) containing a particle. q_{2w} is given by Eq. (14). T_p^n is the temperature of nth particle and $\theta_f(x^n)$ is the fluid temperature at the position of nth particle. Values of $u(x^n)$ and $T_f(x^n)$ at the position of nth particle are obtained by interpolation.

$$q_{2w} = \sum_{n=1}^{N_p}\frac{\mathrm{Nu}}{2}\frac{(\theta_f(\mathbf{x}^n)-T_p^n)}{\tau_T}\delta(\mathbf{x}-\mathbf{x}^n). \tag{14}$$

III. NUMERICAL METHODS AND FLOW CONDITIONS

Isotropic domain with periodic boundary conditions was used for the simulations. Fluid was initially considered to be still with particles homogeneously suspended in the domain. A 128^3 grid size was used and the governing partial differential equations were approximated with a semidiscrete Fourier-Galerkin spectral method, employing exact dealiasing via the 3/2 rule [36]. The resulting partial differential equations were advanced in time using the low-storage, third-order Runge-Kutta scheme described by Spalart *et al.* [37]. The method advanced linear terms implicitly and nonlinear and inhomogeneous terms explicitly.

In order to check the grid resolution, the authors plotted the values of $k_{\max}\eta$ and $k_{\max}\eta_\theta$ with the change of time in Fig. 1. $k_{\max}$ is the maximum wave number of the simulation, η is the Kolmogorov length scale, and η_θ is the temperature microscale. The plot shows that the values of $k_{\max}\eta$ and $k_{\max}\eta_\theta$ are greater than one throughout the simulation. Eswaran and Pope [38] and Balachandar and Maxey [39] showed that values of $k_{\max}\eta$ and $k_{\max}\eta_\theta$ greater than one ensure an accurate resolution of small scale statistics as well as an accurate interpolation of the fluid velocities and fluid temperatures at the particle positions.

Simulations were performed using dual core AMD workstations (3 GHz CPU, 2 GB RAM processor chip) located at the Wayne State University Multi-scale Fluid Dynamics Laboratory. The simulations were terminated after 300 time steps. Nondimensional time step of 0.0009 was used for the time integration.

IV. RESULTS

The effects of volume fraction of nanofluids, size of nanoparticle and the material of nanoparticle are discussed in the sections below. The mechanism of increase of convective heat transfer in nanofluids is also analyzed. The Nusselt number of the fluid was calculated using the formula [31,40] provided in Eq. (15).

$$\mathrm{Nu} = 1 + \frac{\langle u_2\bar{\nabla}T\theta_f\rangle}{\alpha} \tag{15}$$

where α is the thermal diffusivity of fluid.

A. Effect of volume fraction of fluid

To study the effect of the volume fraction of nanofluids on the convective heat transfer rate, the authors performed simulations of Cu(100 nm)/DIW (de-ionized water) and Al_2O_3(100 nm)/DIW nanofluids. The cases used for this study are shown in Table I.

Calculated values of Nusselt number were normalized with the Nusselt number of water. The normalized values (effective Nusselt number) are plotted against the volume fraction of nanofluids in Fig. 2. As observed in previous studies the values of Nusselt number were found to increase with an increase of volume fraction of nanofluids. Figure 2 also shows the effective Nusselt number of Cu(100 nm)/DIW nanofluids at different volume fractions obtained from the

TABLE III. The simulated cases, used for the study of the effect of particle size on the convective heat transfer of nanofluids are shown.

Material	Volume fractions (Φ)	Particle diameter (d)
Cu	0.5%	75 nm, 100 nm, 150 nm
Al_2O_3	0.5%	75 nm, 100 nm, 150 nm

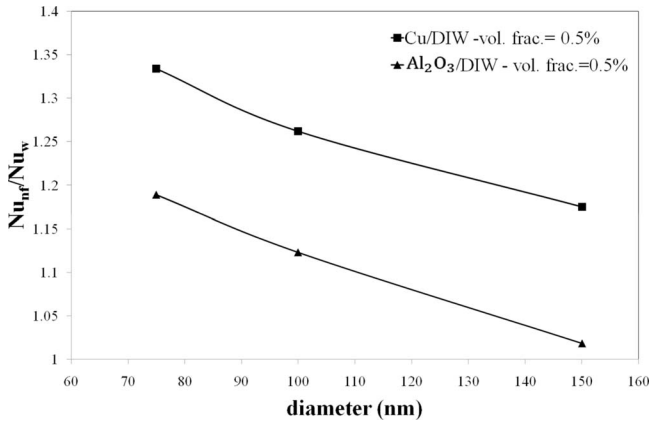

FIG. 6. Effective Nusselt number of Cu/DIW and Al_2O_3/DIW nanofluids, for 0.5% volume fraction, are plotted at different particle sizes. Effective Nusselt number is observed to decrease with the increase of particle diameter.

correlation given in Xuan and Li [17]. The correlation is shown in Eq. (16).

$$\mathrm{Nu}_{nf} = 0.0059(1.0 + 7.6286\Phi^{0.6886}\mathrm{Pe}_d^{0.001})\mathrm{Re}_{nf}^{0.001}\ \mathrm{Pr}_{nf}^{0.4} \tag{16}$$

where Pe_d is the Peclet number, Re_{nf} is the nanofluid Reynolds number and Pr_{nf} is the Prandtl number of nanofluid.

It is evident that the values calculated by the present simulations are comparable with the values obtained from the correlations. The maximum deviation of the present values from that of the correlation is 2.04%. The effective Nusselt number of Cu/DIW nanofluids is greater than that of the Al_2O_3/DIW nanofluids. The effect of the material on the convective heat transfer of nanofluids is discussed later in the paper. One of the drawbacks of the correlation given in Eq. (16) is that the Reynolds number and Prandtl number of nanofluids could not be calculated directly. These values should be obtained from the experimental values of the effective thermal conductivity of nanofluids and the viscosity of nanofluids. These information of Cu(100 nm)/DIW nanofluids could be obtained from Xuan and Li [18]. However no such information is available for Al_2O_3(100 nm)/DIW nanofluids, which prevents the authors from comparing the data obtained from their simulations of Al_2O_3(100 nm)/DIW nanofluids. To observe the effects of Brownian force and thermophoretic force on the Nusselt number of nanofluids, simulations were performed on Cu(100 nm)/DIW nanofluids for 0.1%, 0.5%, and 1.0% volume fractions. It was observed that the Nusselt number (not shown in figure) for these nanofluids was under predicted from about 6–9 % when compared to the present values. It suggests that the nanoparticle forces such as Brownian force and thermophoretic force have significant effect on the convection heat transfer of nanofluids.

It is well known that velocity field influences the gradients in the temperature field and thus can enhance the heat transfer rate in the fluid. In order to study the influence of volume fraction of nanofluids on the velocity field and the temperature gradients, the instantaneous velocity vectors,

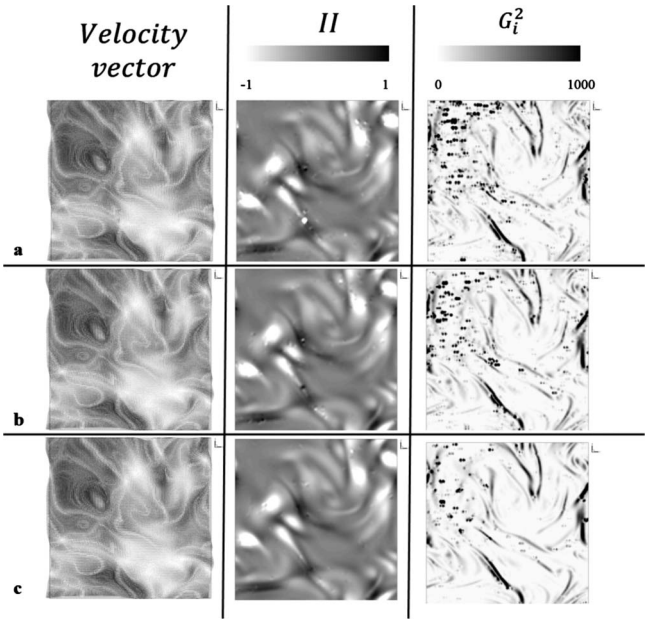

FIG. 7. Contours of instantaneous velocity vector, deformation tensor II and square temperature gradient G_i^2 are shown for 0.5% volume fraction of Cu/DIW nanofluids at different particle diameters. (a) Cu(75 nm)/DIW nanofluid at Φ=0.5%; (b) Cu(100 nm)/DIW nanofluid at Φ=0.5%; (c) Cu(150 nm)/DIW nanofluid at Φ=0.5%. Change in the values of II with the change of the particle diameter is observed to be negligible. However, the contour plot of G_i^2 shows a significant increase in its values as the volume fraction of nanofluids increases.

contour of deformation tensor $II[=(\partial u_i/\partial x_j)(\partial u_j/\partial x_i)]$ and square temperature gradient G_i^2 $(G_i=\partial\theta_f/\partial x_i)$ are plotted in Fig. 3 for Cu/DIW nanofluids at different volume fractions. It is observed that II, which represents the ratio of strength between strain and rotation in the fluid [41], has a large negative value in each of the vortex regions where the velocity vectors exhibit rotational pattern. Change in the value of II with the change of the volume fraction of nanofluids is observed to be negligible. This can be due to the fact that the drag effect of particles of nanofluid on the fluid flow is negligible. However, the contour plots of G_i^2 show a considerable increase in their values as the volume fraction of nanofluids increases. The results suggest that the steep gradients observed in the temperature which increase with an increase in volume fraction of nanofluids, are not influenced by the change in the velocity field.

To achieve further insight into the effect of volume fraction of nanofluids on the values of G_i^2, the transport equation of square temperature gradient has been derived as shown in Eq. (17).

$$\frac{\partial}{\partial t}\left(\frac{1}{2}G_i^2\right) = \underbrace{-\frac{1}{2}S_\theta G_j u_{i,j}}_{P_{c1}} \underbrace{- G_i G_j S_{ij}}_{P_{c2}} \underbrace{+ \alpha\left(\frac{\partial G_i}{\partial x_j}\right)^2}_{\text{Dissipation}} \underbrace{- \alpha\frac{\partial^2}{\partial x_i^2}\left(\frac{1}{2}G_i^2\right)}_{\text{Diffusion}} + \underbrace{(\text{extra term due to particles})}_{P_{c3}}. \tag{17}$$

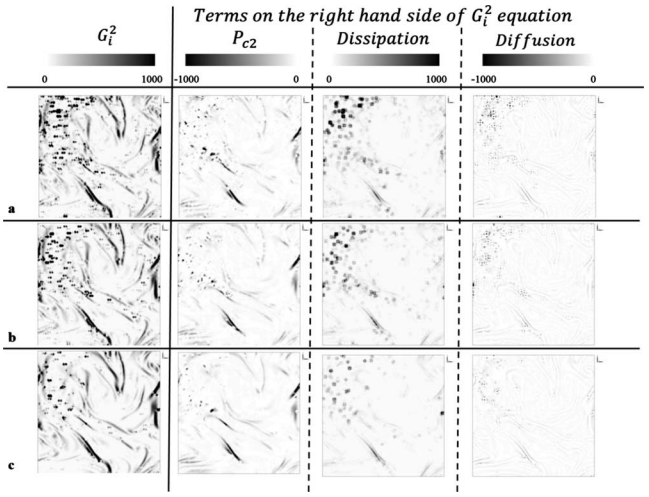

FIG. 8. Distribution of G_i^2 and the terms in the G_i^2 evolution equation; P_{c2}, dissipation and dissipation are shown for (a) Cu(75 nm)/DIW nanofluid at $\Phi=0.5\%$; (b) Cu(100 nm)/DIW nanofluid at $\Phi=0.5\%$; (c) Cu(150 nm)/DIW nanofluid at $\Phi=0.5\%$. The contour of G_i^2 shows a significant decrease in its values for the particle diameter of 150 nm. However, this decrease in the values of G_i^2 is not due to the production term P_{c2}. The magnitude of P_{c2} is not influenced by the increase of the particle diameter.

The first two terms on the right-hand side of the equation are the production caused by the mean temperature gradient, P_{c1} and that generated by the deformation of the velocity field, P_{c2}. Both the production terms are compared and it was observed that P_{c1} remains to be about 1/70 of P_{c2}. Thus the contribution of P_{c1} to the budget of G_i^2 is very low and hence it has not been considered for the study of the effects of various parameters of nanofluids. The last term on the right-hand side of the Eq. (17) represents the influence caused by the two-way interaction between the particles and fluid temperature field to the budget of G_i^2. The increase in the values of G_i^2 with an increase of the volume fraction of fluids can only be caused by two factors, which are (a) the influence of particle dispersion on the fluid velocity field and (b) the influence of two-way interaction between particle and fluid temperature field. It is already shown in Fig. 3 that the influence of particle dispersion on fluid velocity field is very small. Thus the production caused in the values of G_i^2 should be due to the two-way interaction term. Thus the last term on the right-hand side of Eq. (17) is assumed to be a production term and is represented as P_{c3}.

It will be proved from the further examination of contour of each individual term that the assumption made here, by the authors, is right. The term P_{c3} was calculated by subtracting all the others terms on the right-hand side of Eq. (17) from the term on the left-hand side.

Distribution of G_i^2 and the terms in the G_i^2 evolution equation (P_{c2}, dissipation and diffusion) are shown for the Cu(100 nm)/DIW nanofluids at different volume fractions in Fig. 4. It is evident that the increase in the temperature gradients in fluid field with an increase of the volume fraction of nanofluids is not due to the production term P_{c2}. The influence of the volume fraction on the values of P_{c2} is observed very small. Thus the increase in the magnitude of G_i^2 must be due to the term P_{c3}. Figure 5 depicts the distribution of G_i^2 and P_{c3} at different volume fractions of Cu(100 nm)/DIW nanofluids. The values of P_{c3} have both positive and negative values, which are displayed in the left and right hand sides in Fig. 5. Distribution of positive value of P_{c3} is very small and is not significantly influenced by the change of the volume fraction. However, the negative value of P_{c3} is found to be significantly increased with the increase of the volume fraction of nanofluids. Moreover, the high temperature gradients are found to be distributed in the regions of high magnitudes of P_{c3}. Behavior of particles in the regions of high temperature gradients, though is interesting to analyze, is beyond the scope of the present paper. However, Li and Peterson [42], Bleecker *et al.* [43], and Zahmatkesh [44] have all shown that the presence of large temperature gradients influence the movement of particles. Particles usually tend to move away from the region of high temperature gradients.

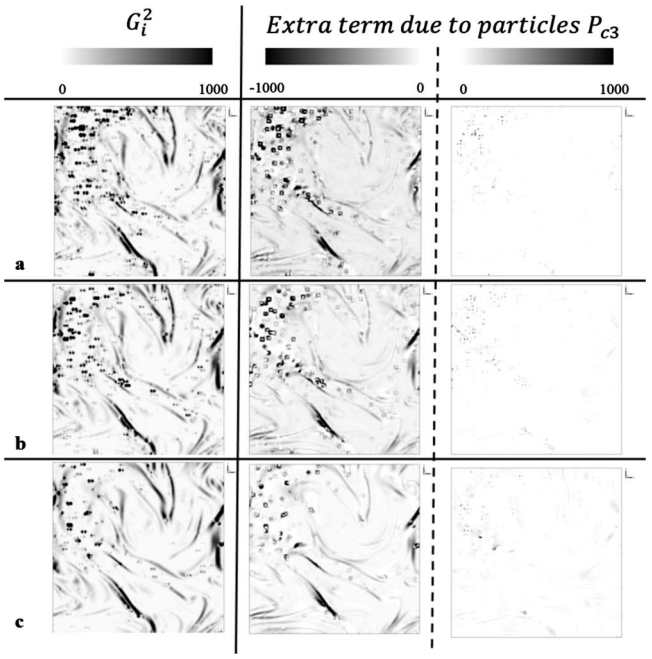

FIG. 9. Distribution of G_i^2 and the negative and positive terms of P_{c3} are shown for (a) Cu(75 nm)/DIW nanofluid at $\Phi=0.5\%$; (b) Cu(100 nm)/DIW nanofluid at $\Phi=0.5\%$; (c) Cu(150 nm)/DIW nanofluid at $\Phi=0.5\%$. Distribution of positive value of P_{c3} is very small and is not significantly influenced by the change of the particle size. However, the negative value of P_{c3} is found to be significantly decreased with the increase of the particle diameter.

Spatial average values of production terms, P_{c2} and P_{c3} are shown in Table II for Cu(100 nm)/DIW nanofluids at different volume fractions. The values are normalized with the value of 0.1% volume fraction case. It can be seen that the average value of P_{c2} decreases with the increase of the volume fraction. It is well known that the increase in the particle volume fraction increases the particle drag, even though it is very small for nanofluids, thus attenuating the turbulence in the fluid. This attenuation of turbulence in the fluid might be causing the decrease in the average value of P_{c2}. However, it was already shown that the influence of particle dispersion on the production of G_i^2 is negligible. The average value of P_{c3} is observed to be increasing steeply with an increase in the volume fraction.

TABLE IV. The normalized spatial average values of G_i^2, P_{c2} and P_{c3}, are shown for different particle diameters of 0.5% volume fraction of Cu/DIW nanofluids. The spatial average values of G_i^2 and P_{c3} are observed to be decreasing and the spatial average values of P_{c2} are found to be increasing with the increase of the particle diameter.

Cu(100 nm)/DIW nanofluid (Φ=0.5%) particle size (d)	$\langle G_i^2\rangle/(\langle G_i^2\rangle)_{75\ \mathrm{nm}}$	$\langle P_{c2}\rangle/(\langle P_{c2}\rangle)_{75\ \mathrm{nm}}$	$\langle P_{c3}\rangle/(\langle P_{c3}\rangle)_{75\ \mathrm{nm}}$
0.1	1	1	1
0.5	0.976	1.021	0.574
1.0	0.841	1.050	0.268

The study of square temperature gradients revealed that the two-way interaction term has very high influence on the temperature fluctuations of the fluid and the temperature fluctuations increase with an increase in the volume fraction. High temperature gradients formed in the fluid cause the water molecules to move away from the region, thus increasing the mixing of the flow and hence increasing the heat transfer rate. These high temperature gradients and fluctuations formed in the fluid with an increase of the volume fraction of nanofluids enhance the heat transfer rate due to mixing, as was observed from the values of effective Nusselt number in Fig. 2.

B. Effect of the particle size

To study the effects of particle size on the convective heat transfer of nanofluids, simulations were performed using Cu and Al_2O_3 nanoparticles suspended in water. The volume fraction of nanofluids used in these simulations is 0.5%. The details of various parameters are tabulated in Table III.

The effective Nusselt number values for various cases shown in Table III are plotted in Fig. 6. The effective Nusselt number value of nanofluids is increased by about 35% in the case of Cu(75 nm)/DIW. However, with the increase in particle diameter, the effective Nusselt number is observed to be decreasing.

In order to observe the effect of particle dispersion on fluid velocity field with the increase of particle diameter, contours of instantaneous velocity vector and II are plotted in Fig. 7. It is evident that the particle dispersion does not affect the fluid field significantly. However, the distribution of G_i^2 shows high temperature gradients in case of Cu(75 nm)/DIW nanofluids. The temperature gradients decrease with an increase of the particle diameter. Decrease in the value of G_i^2 could be due to the decrease in the magnitude of two-way interaction between particle and fluid with the increase of particle size. The values of τ_T are directly proportional to particle diameter. The increase in the value of τ_T should decrease the value of q_{2w} as can be seen from Eq. (13). The distributions of G_i^2, P_{c2}, dissipation term and diffusion term shown in the Eq. (17) are plotted for Cu/DIW nanofluids at different particle sizes in Fig. 8. The influence of particle size on the production term P_{c2} is not significant as has also been observed in the previous section, thus indicating that the influence of particle dispersion on the effective Nusselt number is small.

The values of G_i^2 and P_{c3} are shown for Cu/DIW nanofluids in Fig. 9. P_{c3} is observed to have both positive and negative values. The positive values of P_{c3} which can be considered as the diffusion term has very small values and thus its influence on the G_i^2 can be assumed to be negligible. The negative part of P_{c3}, which acts as production term in Eq. (17) is observed have larger magnitudes at smaller particle diameter. The values of G_i^2 are clearly influenced by the negative part of P_{c3}. The spatial average values of G_i^2, P_{c2}, and P_{c3} are tabulated in Table IV. Number of particles of 150 nm being much smaller than the number of particles of 75 nm (8 times the number of particles for 150 nm case) in 0.5% volume fraction of Cu/DIW nanofluids, turbulence attenuation caused by the 75 nm particles will be higher than the other cases. Thus, the spatial average values of P_{c2} are observed to be decreasing with the decrease of particle size. However, the decrease in the production term with the decrease of particle diameter is significantly lower and does not influence the values of G_i^2. The spatial average values of P_{c2} are clearly increasing with the decreasing particle diameter.

C. Effect of material

The effective Nusselt number plots shown in Figs. 2 and 6 clearly show the effect of material used in the convective

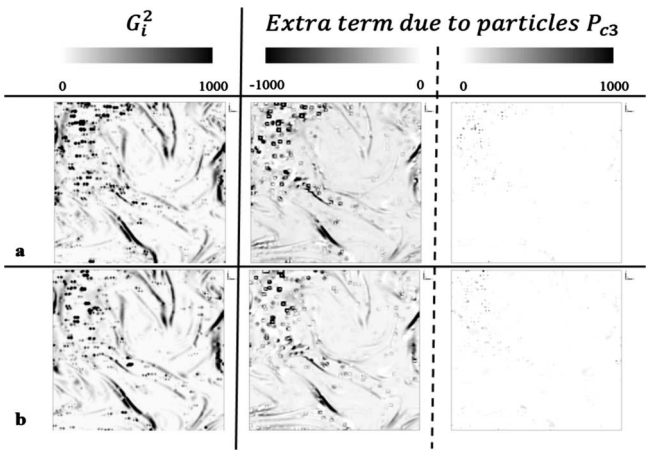

FIG. 10. Distribution of G_i^2 and the negative and positive terms of P_{c3} are shown for (a) Cu(75 nm)/DIW nanofluid at Φ=0.5%; (b) Al_2O_3(75 nm)/DIW nanofluid at Φ=0.5%. Distribution of positive value of P_{c3} is very small and is not significantly influenced by the change of the particle size. However, the negative value of P_{c3} is found to be significantly increased for Cu/DIW nanofluids when compared to that of Al_2O_3/DIW nanofluids.

TABLE V. The normalized spatial average values of G_i^2, P_{c2}, and P_{c3}, are shown here for 0.5% volume fraction of nanofluids of different particle materials. The spatial average values of G_i^2 and P_{c3} are observed to be decreasing and the spatial average values of P_{c2} are found to be increasing for Cu material when compared to the Al_2O_3.

Nanofluid (Φ=0.5%), d=75 nm material	$\langle G_i^2\rangle/(\langle G_i^2\rangle)_{Cu}$	$\langle P_{c2}\rangle/(\langle P_{c2}\rangle)_{Cu}$	$\langle P_{c3}\rangle/(\langle P_{c3}\rangle)_{Cu}$
Cu	1	1	1
Al_2O_3	0.976	1.013	0.589

TABLE VI. Percentage difference in the temperature fluctuations of Cu/DIW and corresponding Al_2O_3/DIW nanofluids.

Nanofluid	θ_f	% enhancement between the corresponding Cu and Al_2O_3 nanofluids
Cu(75 nm)/DIW	0.0837	38.9%
Al_2O_3(75 nm)/DIW	0.0602	
Cu(100 nm)/DIW	0.0627	52.3%
Al_2O_3(100 nm)	0.0412	
Cu(150 nm)/DIW	0.0356	32.8%
Al_2O_3(150 nm)	0.0268	

heat transfer of nanofluids. The effective Nusselt number of nanofluids with Cu nanoparticles was greater than the effective Nusselt number of nanofluids with Al_2O_3 nanoparticles. From the previous sections it is evident that the effect of particle dispersion on convective heat transfer coefficient is negligible. Thus, the authors concentrated only on the P_{c3} term. The distributions of G_i^2 and the negative and positive parts of P_{c3} for Cu(75 nm)/DIW and Al_2O_3(75 nm)/DIW nanofluids reveal that the negative part of P_{c3} is larger for the Cu(75 nm)/DIW nanofluids (Fig. 10). Increase in the values P_{c3} and corresponding increase in temperature gradients in fluid for Cu(75 nm)/DIW nanofluids can also be observed from Table V. The spatial average values of G_i^2, P_{c2}, and P_{c3} show that the spatial average value of P_{c3} of Cu(75 nm)/DIW nanofluids is about 60% larger than that of Al_2O_3(75 nm)/DIW nanofluids. It suggests that the two-way interaction between the fluid and particles in Cu is larger than that of Al_2O_3.

From Eq. (15) it is evident that the values of Nusselt number are strongly dependent on the temperature fluctuations. To observe the effect of material on the temperature fluctuations, the spatial averaged temperature fluctuations are tabulated in Table VI for Cu/DIW and Al_2O_3/DIW nanofluids for different particle sizes. The temperature fluctuations in Cu/DIW nanofluids are observed to be about 1.5 times greater than the corresponding Al_2O_3/DIW nanofluids.

V. CONCLUSIONS

Numerical simulations have been performed by using the Eulerian-Lagrangian method on the convective heat transfer of Cu and Al_2O_3 nanofluids under the turbulent flow conditions. The numerical data calculated for Cu/DIW nanofluids at different volume fractions showed a reasonable match with the correlation data of experiments. The effects of volume fraction of nanofluids, nanoparticle sizes and nanoparticle material were studied. The effective Nusselt number of nanofluids was observed to increase with the increase of nanofluids volume fraction. The study of square temperature gradient evolution equation revealed that the influence of particle dispersion on convective heat transfer of nanofluids is not very significant. Enhancement of Nusselt number in nanofluids is mainly due to the two-way interaction between the fluid and particle temperature. However, the particles used in the simulations were fairly large. Further study using smaller particle diameters is necessary to analyze the effect of particle dispersion on convective heat transfer of nanofluids. The study of particle size effect showed that the effective Nusselt number increases with the decrease of particle size. Two different particle materials used in the simulations (Cu and Al_2O_3) showed that the use of Cu particles in nanofluids was more effective for convective heat transfer when compared to the Al_2O_3 particles.

ACKNOWLEDGMENTS

This work was partially supported by grants from the National Science Foundation (Grant No. ATM-0332910), National Oceanic and Atmospheric Administration (Grant No. NA04OAR4310034), and National Aeronautics and Space Administration (Grant No. NNG04GG46G).

APPENDIX: TURBULENT SCALES

An important concept in turbulent flow is that of energy cascade. That is, the kinetic energy fed to turbulence goes primarily into large eddies, from which it is transferred to smaller eddies, then to still smaller ones, until is dissipated converted to heat by viscous forces. Therefore, within a turbulent flow there exists a spectrum of turbulent eddies. The large eddies have length scales comparable with those of the flow itself [45]. The smallest eddy size in a pipe flow can be given by the equation [45],

$$\eta/l_o \sim \mathrm{Re}^{-3/4}. \tag{A1}$$

Assuming a flow conditions of Re=5500, diameter of pipe (D)=1 mm one gets the value of $\eta \sim 2.5$ μm. Since length scales of the turbulent eddies are larger than the nanoparticle sizes. Thus nanoparticles are transported into the turbulent eddies effectively.

[1] S. U. S. Choi, *Developments Applications of Non-Newtonian Flows*, edited by D. A. Siginer and H. P. Wang (ASME, New York, 1995), Vols. 231: FED and 66: MD, pp. 99–105.
[2] J. A. Eastman, S. U. S. Choi, S. Li, and L. J. Thompson, Proceedings of the Symposium on Nanophase and Nanocomposite Materials II (Materials Research Society, Boston, USA, 1997).
[3] X. Wang, X. Xu, and S. U. S. Choi, J. Thermophys. Heat Transfer **13**, 474 (1999).
[4] S. U. S. Choi, Z. G. Zhang, W. Yu, F. E. Lockwood, and E. A. Grulke, Appl. Phys. Lett. **79**, 2252 (2001).
[5] S. M. S. Murshed, K. C. Leong, and C. Yang, Int. J. Therm. Sci. **47**, 560 (2008).
[6] C. H. Li and G. P. Peterson, J. Appl. Phys. **99**, 084314 (2006).
[7] H. Zhu, C. Zhang, S. Liu, Y. Tang, and Y. Yin, Appl. Phys. Lett. **89**, 023123 (2006).
[8] H. Q. Xie, J. C. Wang, T. G. Xi, Y. Liu, F. Ai, and Q. R. Wu, J. Appl. Phys. **91**, 4568 (2002).
[9] J. A. Eastman, S. R. Phillpot, S. U. S. Choi, and P. Keblinski, Annu. Rev. Mater. Res. **34**, 219 (2004).
[10] Y. Xuan, Q. Li, and W. Hu, AIChE J. **49**, 1038 (2003).
[11] D. Wen and Y. Ding, Microfluid. Nanofluid. **1**, 183 (2005).
[12] Y. Ding and D. Wen, Powder Technol. **149**, 84 (2005).
[13] S. P. Jang and S. U. S. Choi, Appl. Phys. Lett. **84**, 4316 (2004).
[14] S. M. S. Murshed, K. C. Leong, and C. Yang, Appl. Therm. Eng. **28**, 2109 (2008).
[15] C. Nie, W. H. Marlow, and Y. A. Hassan, Int. J. Heat Mass Transfer **51**, 1342 (2008).
[16] S. Kondaraju, E. Jin, and J. S. Lee, Int. J. Heat Mass Transfer (to be published).
[17] Y. Xuan and Q. Li, ASME J. Heat Transfer **125**, 151 (2003).
[18] Q. Li, Y. Xuan, J. Jiang, and J. W. Xu, J. Astronaut. Sci. **26**, 391 (2005).
[19] Y. Yang, Z. G. Zhang, E. A. Grulke, W. B. Anderson, and G. Wu, Int. J. Heat Mass Transfer **48**, 1107 (2005).
[20] S. E. B. Maiga, C. T. Nguyen, N. Galanis, and G. Roy, Superlattices Microstruct. **35**, 543 (2004).
[21] S. E. B. Maiga, S. J. Palm, C. T. Nguyen, G. Roy, and N. Galanis, Int. J. Heat Fluid Flow **26**, 530 (2005).
[22] Y. He, Y. Men, Y. Zhao, H. Le, and Y. Ding, Appl. Therm. Eng. **29**, 1965 (2009).
[23] S. Kondaraju, X. Xu, and J. S. Lee, Int. J. Numer. Methods Fluids (to be published).
[24] M. R. Maxey and J. J. Riley, Phys. Fluids **26**, 883 (1983).
[25] A. Li and G. Ahmadi, Aerosol Sci. Technol. **16**, 209 (1992).
[26] L. Talbot, R. K. Cheng, R. W. Schefer, and D. R. Willis, J. Fluid Mech. **101**, 737 (1980).
[27] G. S. McNab and A. Meisen, J. Colloid Interface Sci. **44**, 339 (1973).
[28] S. K. Das, S. U. S. Choi, W. H. Yu, and T. Pradeep, *Nanofluids: Science and Technology* (Wiley, Hoboken, NJ, 2008).
[29] K. Apostolou and A. N. Hrymak, Comput. Chem. Eng. **32**, 841 (2008).
[30] A. Pumir, Phys. Fluids **6**, 2118 (1994).
[31] V. Borue and S. A. Orszag, J. Sci. Comput. **12**, 305 (1997).
[32] D. Lohse and F. Toschi, Phys. Rev. Lett. **90**, 034502 (2003).
[33] O. Zikanov and A. Thess, Appl. Math. Model. **28**, 1 (2004).
[34] C. Rosales and C. Meneveau, Phys. Fluids **17**, 095106 (2005).
[35] S. Sundaram and L. R. Collins, J. Fluid Mech. **379**, 105 (1999).
[36] C. Canuto, M. Y. Hussaini, A. Quarteroni, and T. A. Zang, *Spectral Methods in Fluid Mechanics* (Springer, New York, 1987).
[37] P. R. Spalart, R. D. Moser, and M. M. Rogers, J. Comput. Phys. **96**, 297 (1991).
[38] V. Eswaran and S. B. Pope, Comput. Fluids **16**, 257 (1988).
[39] S. Balachandar and M. R. Maxey, J. Comput. Phys. **83**, 96 (1989).
[40] E. Calzavarini, C. R. Doering, J. D. Gibbon, D. Lohse, A. Tanabe, and F. Toschi, Phys. Rev. E **73**, 035301(R) (2006).
[41] T. Yano and N. Kasagi, JSME International Journal Series B, **42**, 284 (1999).
[42] C. H. Li and G. P. Peterson, Adv. Mech. Engg., 2010 (2010).
[43] K. De Bleecker, A. Bogaerts, and W. Goedheer, Phys. Rev. E **71**, 066405 (2005).
[44] I. Zahmatkesh, Int. Commun. Heat Mass Transfer **35**, 369 (2008).
[45] S. B. Pope, *Turbulent Flows* (Cambridge University Press, Cambridge, England, 2000).